Hindawi
Advances in Materials Science and Engineering
Volume 2021, Article ID 4318993, 17 pages
https://doi.org/10.1155/2021/4318993

Research Article

The Equilibrium Time and Salt Expansion Characteristic of Sulfate Saline Soil upon Cooling

Yanjie Ji,[1] Xu Li ,[1] Wei Wang,[2] and Li Liu[1]

[1]*Key Laboratory of Urban Underground Engineering of Ministry of Education, Beijing Jiaotong University, Beijing, China*
[2]*China Hebei Construction and Geotechnical Investigation Group Ltd., Shijiazhuang 050227, China*

Correspondence should be addressed to Xu Li; 19115023@bjtu.edu.cn

Received 4 November 2021; Accepted 25 November 2021; Published 13 December 2021

Academic Editor: Bingxiang Yuan

The salt expansion disease is severe for the soil containing sodium sulfate in cold regions. This paper carried out one-dimensional salt expansion tests of saline soil, the crystallization test of saturated sodium sulfate solution, and the numerical cooling tests to explore the stability time of the salt expansion test and determine the standard procedure of salt expansion tests. The test results demonstrate that (i) the temperature equilibrium and the crystallization process are almost simultaneously completed in both sulfate saline soil and sulfate solution upon cooling; (ii) referring to the deformation equilibrium standard used in soil consolidation test, an expansion rate of less than 0.02 mm/h is suggested in the saline expansion test; and (iii) the equilibrium time is found to have a quadratic polynomial relationship to sample size and is much shorter under liquid bath conditions than under gas bath conditions. Based on these findings, a standard procedure of the one-dimensional salt expansion test is proposed, in which the test equipment, the test process, the deformation stabilization time of salt expansion, and the data processing method are provided. As the deformation and the temperature are synchronized, the deformation stabilization time of samples with different sizes in different cooling media is recommended.

1. Introduction

Saline soil is widely distributed in northwestern China [1]. In the northwestern region, the sulfate crystallization effect and chemical reactions between sulfate and building materials will cause damage to building foundations, pile structures [2, 3], and slope structures [4]. The soil is defined as saline soil with soluble salt content equal to or greater than 0.3% [5]. The subgrade composed of sulfate saline soil is more vulnerable to diseases, such as dissolution, salt heave, frost heave, and mud boiling, among which the salt heave is the most severe disease [6]. With the development of the "Belt and Road Initiative" development strategy, the salt expansion problem has brought great harm to the engineering construction industry and has attracted more attention from the engineering and academic industry.

The solubility of sodium sulfate decreases sharply with a decrease in the environmental temperature, accompanied by the salt crystallization and salt swelling effect in sulfate saline soil. According to the solubility of sodium sulfate, the salt swelling effect mainly occurs at the temperature stage above 0°C. The solubility of sodium sulfate is shown in Figure 1. The salt crystallization behavior is driven by the temperature difference between daytime and nighttime, and such dissolution effect may easily cause engineering diseases in the continuous salt swelling-collapse process. To better illustrate the temperature effect on the salt expansion process, Lai et al. [7] and Wan et al. [8, 9] conducted salt expansion experiments with different cooling rates. In conclusion, with an increased initial concentration of sulfate content, the cooling rate is slowed down, followed by decreased maximum supersaturation rate, increased salt crystallization rate, and higher salt expansion rate. Some researchers [9, 10] also obtained the initial crystallization temperature of soils with different salt concentration contents through experiments. Xiao et al. [11] derived the liquid water content of sulfate saline soil based on the thermodynamic theory. Fang et al. [12] derived the theoretical crystallization amount of

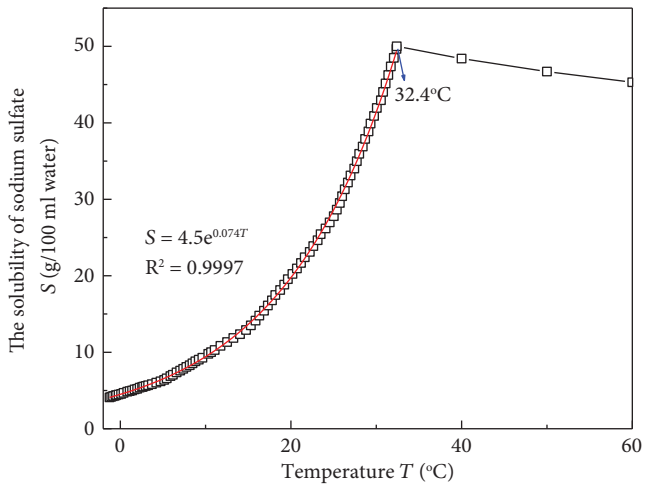

Figure 1: The solubility of sodium sulfate.

Glauber's salt in saline soil at different temperatures and established an empirical model for salt expansion. Zhang et al. [13] established a four-field coupling model of hydrothermal, mechanical, and salt fields. Bai et al. [14, 15] studied the constitutive model of geomaterials with thermal effects. Some researchers [16–20] have conducted salt expansion tests to investigate influencing factors of salt expansion, such as salt type, salt content, water content, temperature, cooling rate, initial dry density, soil type, attached load, and water supplement. However, in a closed system, the salt expansion is driven by temperature. How the salt crystallization effect developed after environment temperature is stabilized and whether the salt expansion effect is synchronized with stabilized soil temperature still remain unclear. With controlled cooling conditions and sample size, there is still no clear specification for the sample's temperature stabilization time, sample's temperature stability, and the stability standard of deformation. This paper summarizes and compares the test instruments, test procedures, and test programs from previous studies to explore a more reasonable salt expansion test method.

There are mainly three types of test equipment reported in the literature: a typical salt expansion test device [21] that is similar to the consolidation test device, as shown in Figure 2(a), a cylindrical-shaped confined one-dimensional salt expansion test device [22], as shown in Figure 2(b), and (iii) a model test device of salt expansion [23], as shown in Figure 2(c). As a model test device, the sample volume is large. During the cooling stage, the problem can be complicated by the water and the salt migration caused by the difference in the soil's internal temperature [24–28].

An essential influencing factor to the salt expansion test is the temperature stabilization time [29–32]. The stabilization time is dependent on the soil size and the cooling pattern [20]. Previous studies [8, 33] set each testing stage (with a change of temperature level) as lasting from 2 to 8 hours. The salt swelling development is insufficient when the stabilization time is short. However, test efficiency is low when the stabilization time is extended. Hence, it is necessary to balance and determine a reasonable salt swelling stability time. However, there still lacks a criterion for the stabilization time in the salt expansion test. To fill this gap, both laboratory tests and numerical tests are carried out in this study.

The primary purpose of this study is as follows: (a) Determine whether the deformation stabilization time and the temperature stabilization time of saline soil are synchronized. (b) Determine the deformation stabilization time of the salt expansion test. (c) Determine the effect of cooling rate and cooling method on salt expansion. (d) Summarize the standard experimental procedure of salt expansion experiment for future study.

2. Experimental Study on the Salt Expansion

2.1. Purpose. It is well known that the water and salt migration can cause continuous deformation of the sulfate saline soil upon temperature gradient [34, 35]. To decouple the local element behavior and the migration behavior, the element test methodology is used in this study. In this element test, the testing system is closed without water and salt supply or discharge. The element test can simplify the problem, and the test results can be used to develop a constitutive model for the sulfate salt soil. Combining this constitutive model and the salt migration simulating tool, a complete simulation of the salt expansion process can be well simulated.

In this study, only soil element tests are considered. In the element test, the salt or water migration effect in the salt expansion process is minimized as much as possible and is ignored. In an element test, the soil sample is embedded in a closed system. When the soil's water content remains unchanged in this closed system, the salt crystallization is only related to the temperature and the testing time. A series of laboratory tests are carried out to study the effect of temperature and time on the salt expansion process and to determine whether the temperature of the soil sample and the salt expansion deformation simultaneously and directly affect the salt expansion test process. This paper carried out a one-dimensional salt expansion soil element test to explore the relationship between the soil temperature and the salt expansion behavior.

2.2. Test Materials and Test Plan. This paper takes Qinghai silty clay as the research object and uses distilled water to clean the salt in Qinghai silty clay. The soil particles of Qinghai silty clay are summarized as follows: liquid limit (ll) = 27.15%; plastic limit (pl) = 15.10%; plasticity index (PI) = 12.05; soil's maximum dry density = 1.75 (g/cm^3); optimal moisture content = 15.50%. The specific gravity of the soil (Gs) is 2.67. The soil grain size distribution curve is illustrated in Figure 3.

Regarding the test plan, the salt expansion's sensitive temperature range is mainly determined by the soil's initial salt concentration. In the outdoor salt expansion test [36], salt expansion's sensitive temperature range is from 18°C to 0°C. Therefore, the temperature for this study is 25°C–1°C.

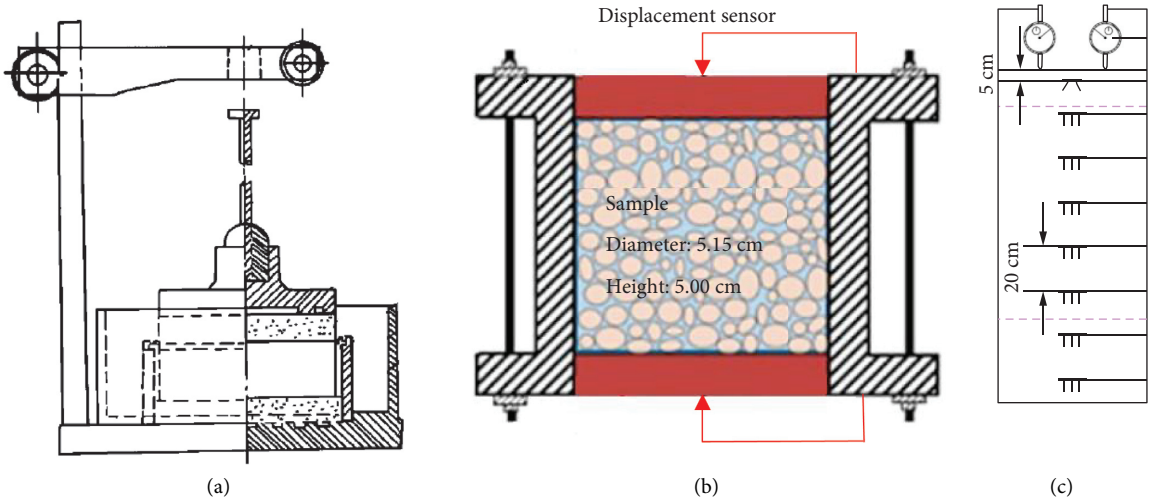

Figure 2: One-dimensional salt expansion test device in literature. (a) Schematic diagram of salt heaving test device under pressure condition [21]; (b) 1D lateral limit unit salt expansion test device [22]; (c) salt expansion model test device [23].

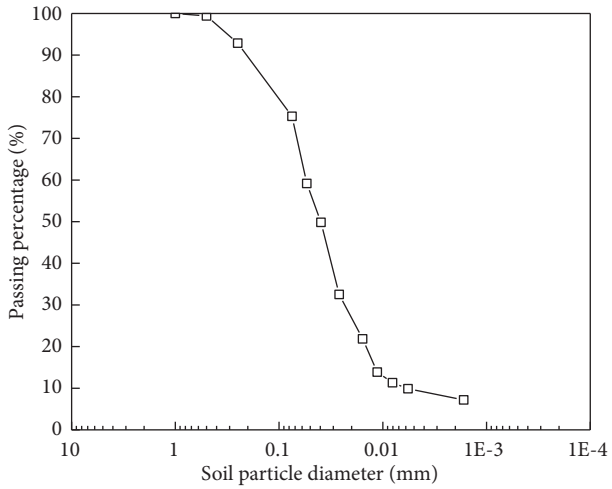

Figure 3: Grain size distribution of soil.

This test uses a sodium sulfate solution with a concentration of 1.6 mol/L to mix the soil according to the set water content (15.50%). The sodium sulfate solution is mixed with testing soil in a sealed bag and put in a thermostat for curing at 25°C for 24 hours before pressing the specimen to reach dry density status. The salt content of soil samples is 3.52%. The test plan is shown in Table 1. There are in total 1 big sample (Test No. B1) and 9 small samples (Test No. S1–S9) used in the test. A special device is designed (will be described in the following section) and applied to a big sample (B1) to check the equilibrium time of the soil's center. Eight small samples (S1 to S8) were tested to check the characteristics of the salt expansion behavior. Another small sample S9 was tested to obtain the equilibrium time for salt expansion of the specimen under liquid bath conditions.

2.3. 1D Salt Expansion Test of Big-Size Samples

2.3.1. Test Device. The test device used for big-size samples includes the salt expansion test barrel, DT85, PT100 temperature sensor, and the digital dial indicator, as shown in Figure 4. In this test, a C4-600 programmable constant temperature test chamber is used to maintain the cooling environment. The sample is put into the thermostat and cooled by the air from all directions. During the test process, both the temperature and displacement of the soil sample are monitored.

2.3.2. Test Procedure. The one-dimensional salt expansion soil column test procedure is as follows. First, the test barrel's sidewall is a coat with petroleum jelly, and a fresh-keeping

Table 1: 1D test plan for salt expansion of Qinghai silty clay.

Test number	Degree of compaction	Sample size	The cooling rate of an incubator	Cooling method
B1	0.95	$H = 11.59$ cm and $D = 17.90$ cm	1°C/min	Air bath
S1, S2, S3, and S4	0.84, 0.89, 0.93, and 0.97	$H = 4.00$ cm and $D = 6.18$ cm	1°C/min	Air bath
S5, S6, S7, and S8	0.84, 0.89, 0.93, and0.97	$H = 4.00$ cm and $D = 6.18$ cm	1°C/h	Air bath
S9	0.95	$H = 3.91$ cm and $D = 8.00$ cm	—	Liquid bath

Note. The critical crystallization temperature of samples B1 and S1–S8 was 22°C. The critical crystallization temperature of sample S9 was 20°C.

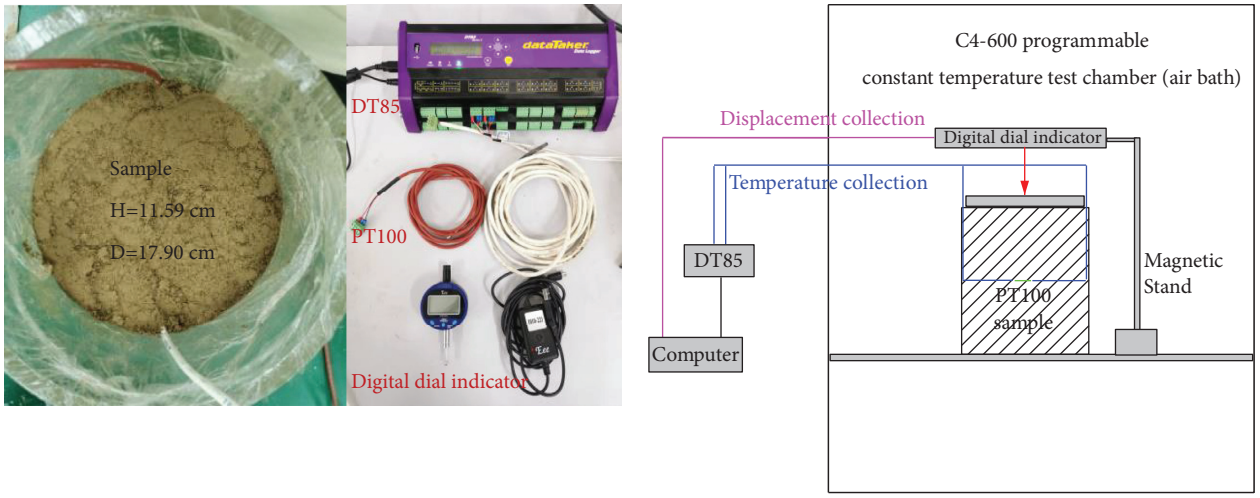

(a) (b)

Figure 4: 1D salt expansion test device for big-size sample. (a) Sample and temperature sensor; (b) schematic diagram of the test device.

film is covered to reduce the influence of sidewall friction. The soil sample is compacted in six layers, two PT100 temperature sensors are embedded in the center of the third and fourth layers of the sample, and the temperature of the center point of the soil is collected every 1 minute by DT85. A digital dial indicator is installed on the top of the sample and collected every 1 minute. The C4-600 programmable constant temperature test chamber can realize the automatic constant temperature function by air bath. The test takes 25°C ⟶ 12°C ⟶ 8°C ⟶ 4°C as the cooling gradient, and the cooling rate of the incubator is 1°C/min. The sample is cured at 25°C for 24 h and then cooled to 12°C, and after the constant temperature for 24 h, it decreases to the next level of temperature at the same cooling rate. In the whole process of the test, DT85 collects the sample's center temperature in real-time and counts the salt expansion deformation of the soil sample collected by the dial indicator.

2.4. 1D Salt Expansion Test of Small-Size Samples

2.4.1. Test Device. The test device used for small-size samples includes the cutting ring with a diameter of 6.18 cm and a height of 4.00 cm, the vernier caliper, and the C4-600 programmable constant temperature test chamber, as shown in Figure 5. In this test, the small-size samples are put into the calorstat and cooled by the air from all directions. After the test is completed, its deformation is measured, and the temperature at the final equilibrium state is recorded.

2.4.2. Test Procedure under Air Bath Condition. The one-dimensional salt expansion test procedure is as follows. The C4-600 programmable constant temperature test chamber can automatically adjust the temperature change according to the set cooling program. The test uses 25°C ⟶ 12°C ⟶ 8°C ⟶ 4°C ⟶ 1°C as the cooling gradient. The cooling rate of the incubator cooling stage is set according to the test plan. The sample is cured at 25°C for 24 h, and the temperature is reduced to 12°C at the set cooling rate. After a constant temperature of 24 h, it will also drop to the next level of temperature at the set cooling rate. At each level of the constant temperature, the sample will be measured by vernier calipers at a predecided time interval (usually 2–4 h), and the circumference of the cutting ring will be divided into three parts. The average value of the three measurements is taken as a result to reduce error. After the test, the testing sample is immediately put back into the incubator, and the environment temperature is adjusted to the next temperature level after the deformation is stabilized to ensure that the sample's sodium sulfate is sufficient during the cooling process crystallization.

2.5. 3D Salt Expansion Test of Small-Size Samples

2.5.1. Test Device. A liquid bath is more efficient compared to an air bath as it can reduce the equilibrium time in the salt expansion test. To study this effect, another device with a liquid bath environment is used in the 3D salt expansion test, as shown in Figure 6.

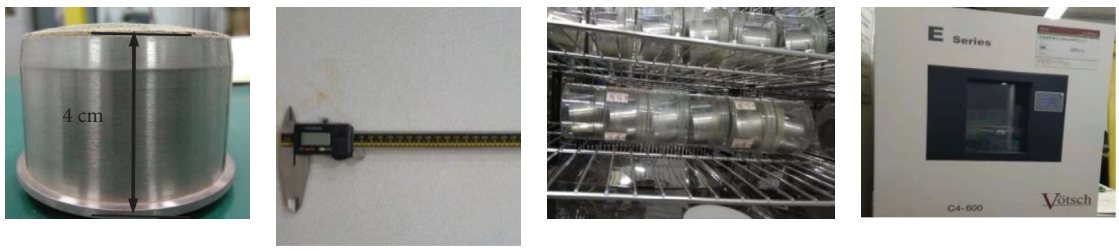

(a) (b) (c) (d)

Figure 5: 1D salt expansion test for the small-size sample under air bath condition. (a) Sample S1 after salt expansion; (b) vernier caliper; (c) samples in the C4-600 programmable constant temperature test chamber; (d) C4-600 programmable constant temperature test chamber.

2.5.2. Test Procedure under Liquid Bath Condition. The three-dimensional salt expansion test procedure is as follows. The sample was made at room temperature above 25°C, and then it was placed in a temperature-controlled shaft chamber. The test was set up with an envelope pressure of 0 kPa, and the temperature of the specimen was controlled by a Thermo cold bath. PT100 is placed inside the chamber of the temperature-controlled body changer. The DT85 was used to collect the data on the internal temperature of the chamber. The test uses 20°C ⟶ 12°C ⟶ 8°C ⟶ 4°C ⟶ 1°C as the cooling gradient. When the drainage in the chamber is <0.2 mL/h, the sample deformation is considered to be stable, and the test reaches an equilibrium state. After reaching equilibrium, total outflow, which is major caused by the swelling of the soil sample, is recorded as ΔV_0. The volume change of water and chamber caused by the temperature change is calibrated in advance and recorded as ΔV_2. Hence, the volume change of salt swelling of the sample is $(\Delta V_0 - \Delta V_2)$.

3. Test Results on the Equilibrium Time

3.1. Result Analyses. The test results of the 1D salt expansion test for big-size samples are shown in Figure 7. The critical crystallization temperature of the soil sample is 22°C, calculated from the solubility of sulfate. It can be seen from Figure 7 that the initial expansion temperature of the sample is 22°C and the salt expansion height of the soil sample increases with the decrease of the temperature. The temperature and the salt expansion are both stable. It can be concluded that after the salt in the soil sample solution reaches saturation, the salt will precipitate as the temperature decreases, and the crystallization is completed when the temperature is stable; thereby, there is a good correspondence between the deformation and the temperature.

The test results of the 1D salt expansion test of small-size samples are shown in Figure 8. It can be seen from Figure 8 that the salt expansion rapidly developed in the initial cooling stage, that is, within 2–4 hours after the thermostat reaches the predecided temperature level. As the time increased, the salt expansion slowed down and gradually stabilized.

The test results of the 3D salt expansion test of small-size samples under the liquid bath are shown in Figure 9. The volume change ΔV_0 caused by the temperature decrease is a combined reflection of the sample's salt expansion and the water volume contraction within the axial chamber. The volume change ΔV_2 (0 mL ⟶ −0.61 mL ⟶ −1.06 mL ⟶ −1.12 mL ⟶ −1.39 mL) of the water inside the chamber due to the temperature decrease (20°C ⟶ 12°C ⟶ 8°C ⟶ 4°C ⟶ 1°C) can be obtained through the calibration test with iron instead of the sample. The sample's volume of salt expansion is ΔV_0 minus ΔV_2. Figure 9 illustrates that the sample's volume expands when the temperature decreases and the deformation stabilizes when the temperature is stable.

3.2. A Proposition on the Equilibrium Time and Its Verification. In the last section, the test results in Figure 7 show that the salt expansion (hence also salt crystallization effect) and temperature equilibrium are cotranscriptionally occurring. In this section, the point of salt crystallization effect and temperature equilibrium cotranscriptionally occurring will be proved through the crystallization test in solution.

The specific work is as follows. We prepare a sodium sulfate solution with a concentration of 1.6 mol/L (the concentration is the concentration of sodium sulfate saturated solution at 22°C), as shown in Figure 10(a). Then, we seal it with the cling film and place it in a thermostat at 12°C to cool down. A thermometer is used to measure the temperature of the solution every few minutes and record the crystallization of the solution with photos, as shown in Figures 10(b)–10(d). When the solution's temperature reaches 12°C, the clear solution obtained by the filtration is shown in Figure 10(e), and the crystals are shown in Figure 10(f). The filtered material is weighed and dried to obtain the salt and water quality in the filtered material at this time. When the solution temperature reaches 12°C, the crystallization completion rate is 99%. The calculation table is shown in Table 2. The filtered solution was sealed under plastic wraps and placed in a thermostat at 12°C. The reproduced crystals were low.

It can be seen that when the temperature of the solution reaches the saturation temperature, as the temperature decreases, crystallization occurs, the temperature is stable, and the crystallization is completed. It further explains why

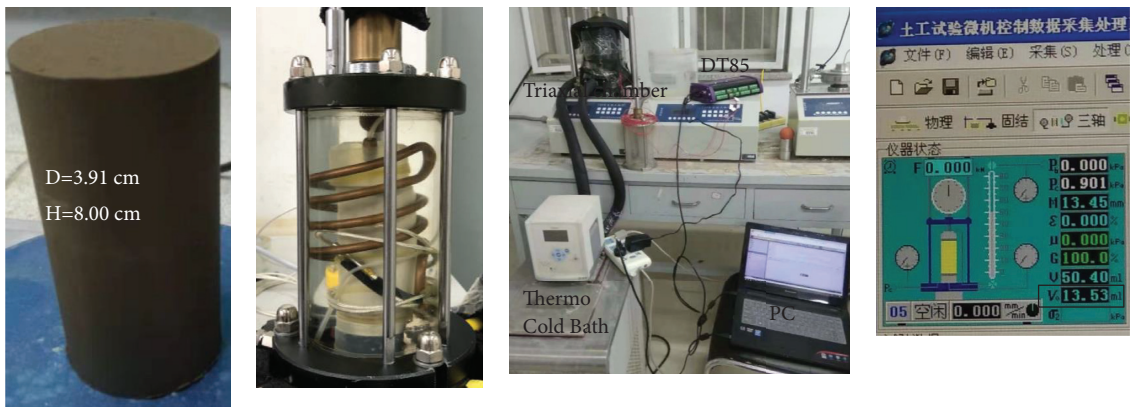

FIGURE 6: 3D salt expansion test for the small-size sample under liquid bath condition. (a) Sample; (b) sample in chamber; (c) test equipment diagram; (d) data acquisition interface.

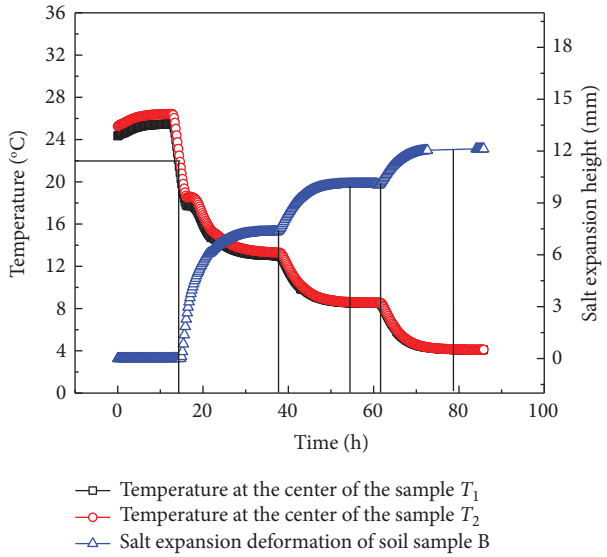

FIGURE 7: Variation of sample height and temperature at the sample center (big-size sample).

the salt expansion is also stable when the soil sample temperature is stable in Section 3.1. Figure 11 illustrates that, during the cooling process, the supersaturation of the solution is relatively high, and the crystals formed are in the shape of small rods. When the solution's temperature is constant, the solution's supersaturation is small, and the resulting crystals are lumpy. As shown in Figure 11, when the cooling rate of the soil is low, the crystal form will be more stable, and its salt expansion rate will be comparatively larger.

3.3. Effect of Cooling Gradient on the Expansion Rate. Qinghai silty clay was used for the salt swelling test to explore the effect of cooling rate on salt swelling. The water content was maintained, and the cooling rate of the incubator was controlled at 1°C/min and 1°C/h. The test results are shown in Figure 12.

When the water content and the degree of compaction are under the same level, the salt expansion rate of the Qinghai silty clay shows an increasing tendency with the decrease of the cooling rate. Wan et al. [8] found that the salt expansion rate of sulfate saline soil increased with a reduced cooling rate through the one-dimensional salt expansion test under closed conditions. As the cooling rate decreases, the water and salt migration behavior become more distinct. The migration of salt and water leads to the accumulation of crystals and more significant salt swelling and deformation. On the microscopic level, it is the change of soil pore structure [37–40]; secondly, the smaller the cooling rate, the more stable the crystal morphology [41, 42]. In summary, the lower the cooling rate, the greater the salt expansion rate. Hence, to avoid water and salt migration and to obtain a uniform unit, it is recommended to cool down quickly.

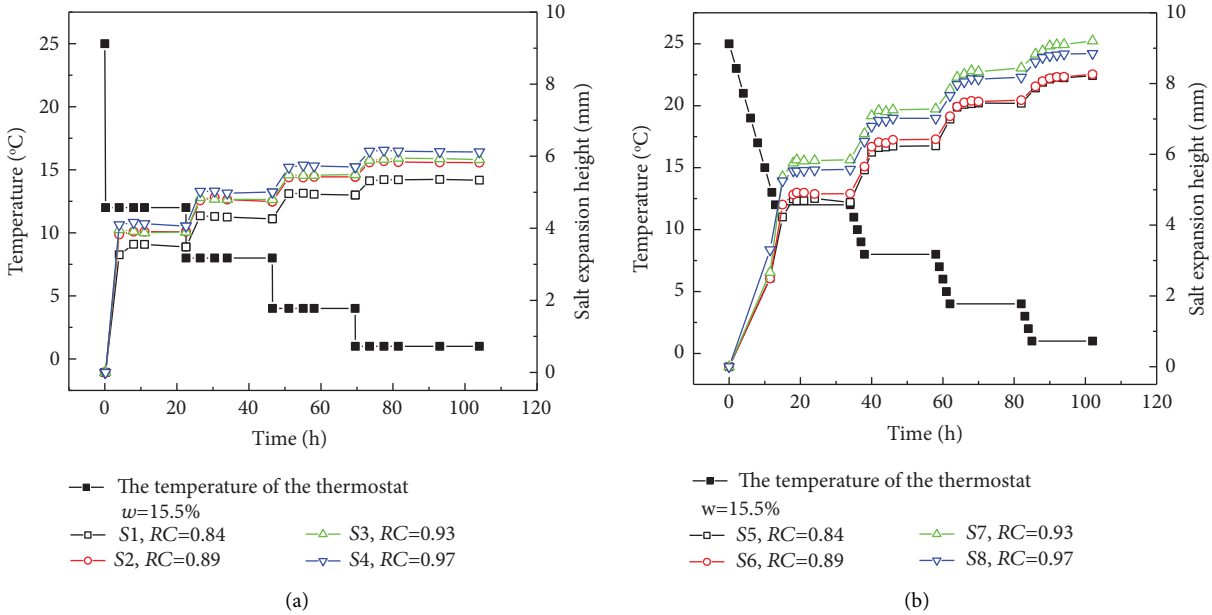

FIGURE 8: Swelling process in 1D salt expansion test with air cooling condition (small-size samples). (a) Cooling rate of incubator 1°C/min; (b) cooling rate of incubator 1°C/h.

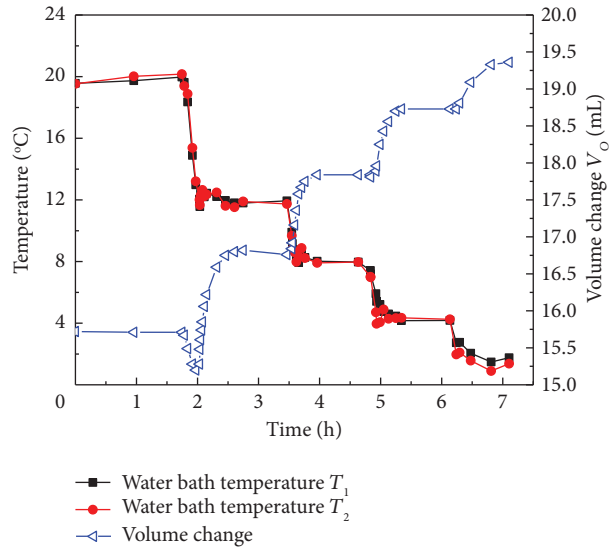

FIGURE 9: Swelling process in 3D salt expansion test with liquid cooling condition (small-size samples).

3.4. Effect of Cooling Gradient on the Equilibrium Time. From the salt swelling deformation curve with time, we derive the time to obtain the soil sample's salt swelling rate with the time curve, taking 8°C and 1°C as examples, as shown in Figures 13–16. Then, the salt swelling stability standard and the salt swelling stability time can be obtained.

Because the salt swell test is similar to the consolidation test, the salt swelling test's deformation stability standard can be formulated by analogy with the consolidation test. The consolidation test's loading method is unidirectional, and the sample size is 61.8 mm in diameter and 20 mm in height. The consolidation test's stability standard [43] is as follows: the deformation per hour in each pressure level is not more than 0.01 mm, or the consolidation time is 24 hours. The salt expansion test is a two-way expansion under confined conditions, and the sample size is 61.8 mm in diameter and 40 mm in height. Therefore, the salt expansion test's stability standard is as follows: the deformation per hour at each temperature is not more than 0.02 mm, or the temperature is stable for 24 hours.

Figures 13 and 15 show that the soil sample is deformed and stabilized at 12°C and then cooled to 8°C. The critical crystallization temperature of the soil sample is 12°C. The temperature completion rate is the ratio of the difference between the soil sample's central point temperature and the initial ambient temperature to the difference between the set

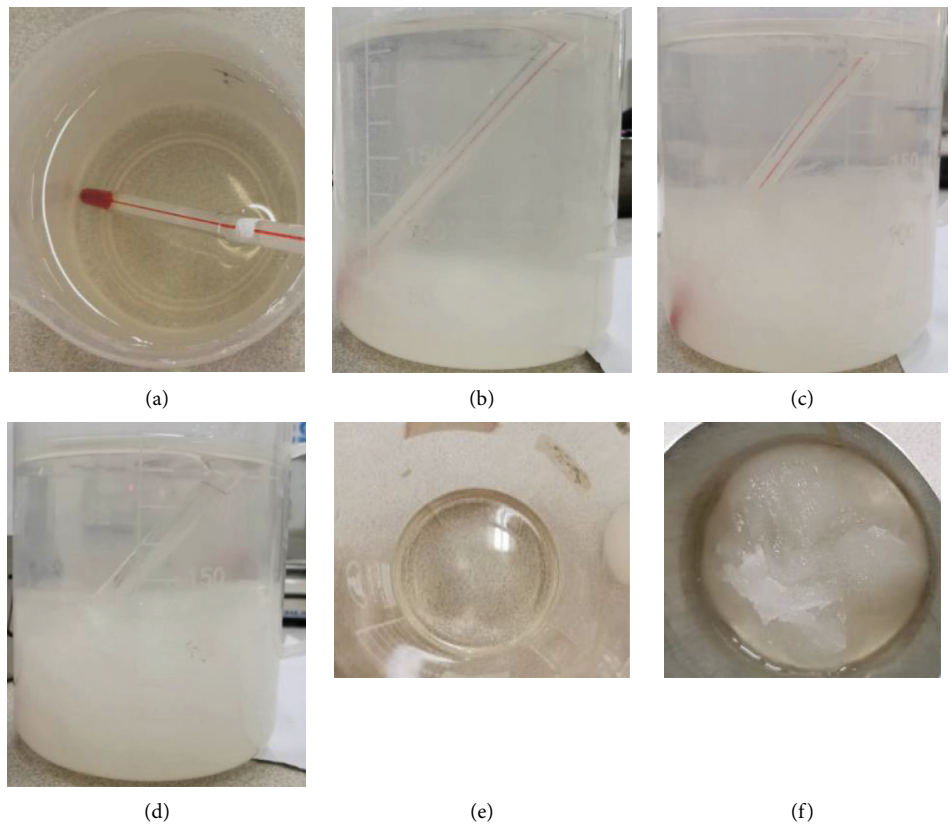

(a) (b) (c)

(d) (e) (f)

Figure 10: The crystallization process of 1.6 mol/L sodium sulfate solution. (a) 0 minutes, 25°C; (b) 12 minutes, 20°C; (c) 50 minutes, 16°C; (d) 120 minutes, 12°C; (e) clear solution after filtration; (f) crystalline after filtration.

Table 2: Calculation of crystallization completion rate when the solution temperature reaches 12°C.

The mass of water in the initial solution (g)	The mass of salt in the initial solution (g)	Quality of dry salt in the filter material (g)	The quality of water in the filter material (g)	The mass of sodium sulfate in the crystal (g)	The quality of theoretical crystalline sodium sulfate (g)	Actual crystallization completion rate
228.26	51.86	37.90	103.26	30.34	30.63	0.99

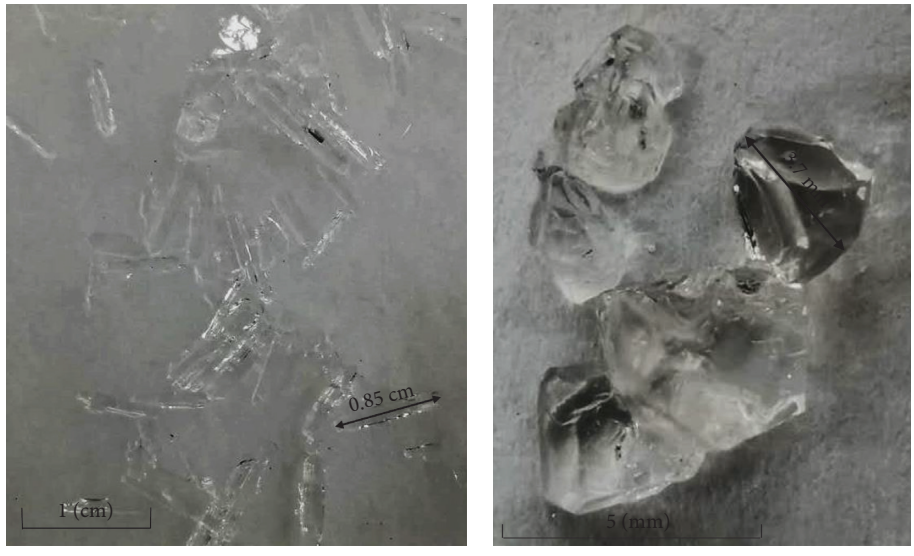

(a) (b)

Figure 11: Crystalline diagram. (a) Rod-shaped crystals during two hours of cooling process from 25°C to 12°C; (b) block crystal after twelve hours of constant temperature process at 12°C.

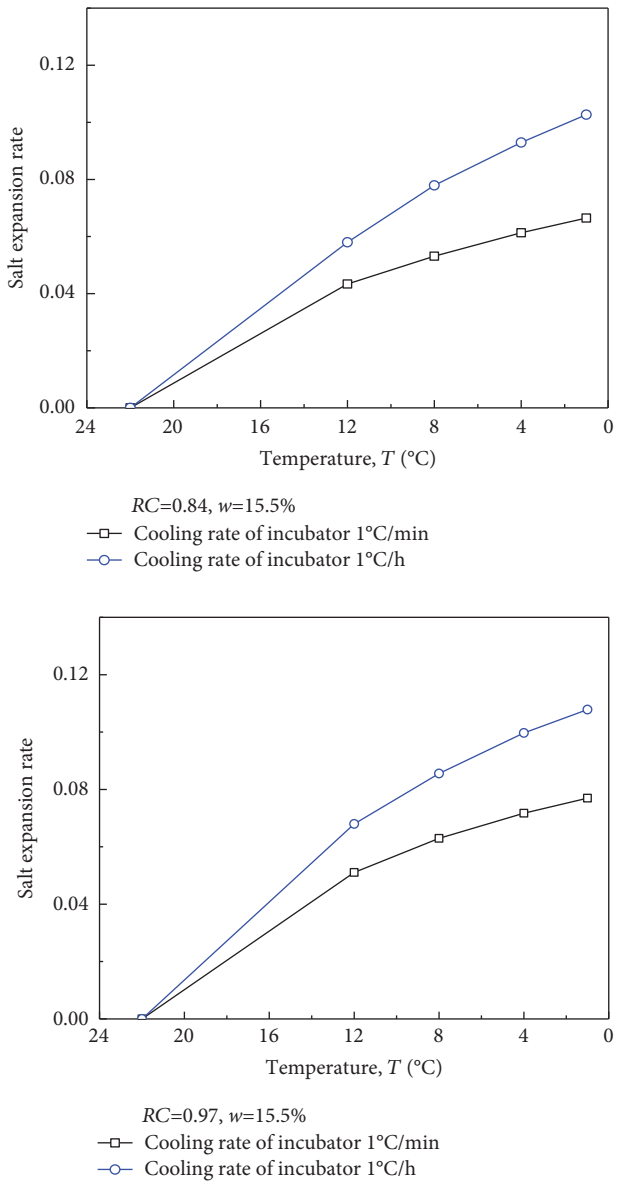

Figure 12: The salt expansion rate of Qinghai silty clay with temperature.

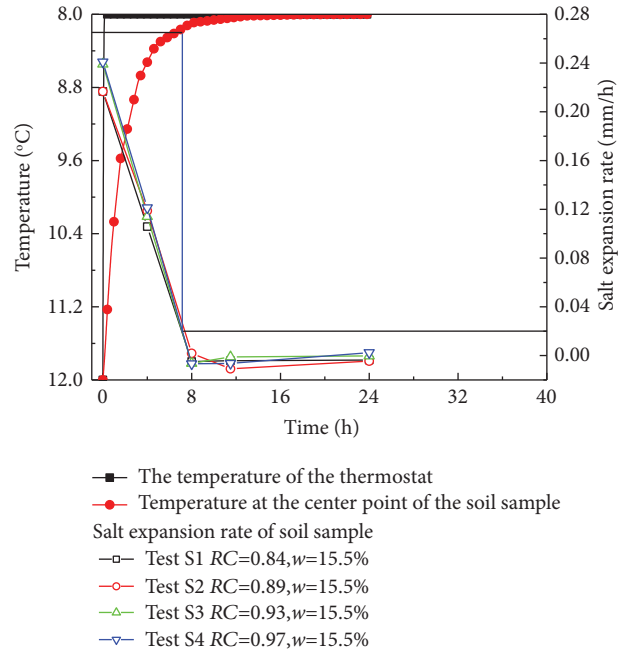

Figure 13: Soil sample swelling rate versus time at 8°C with a cooling rate of 1°C/min.

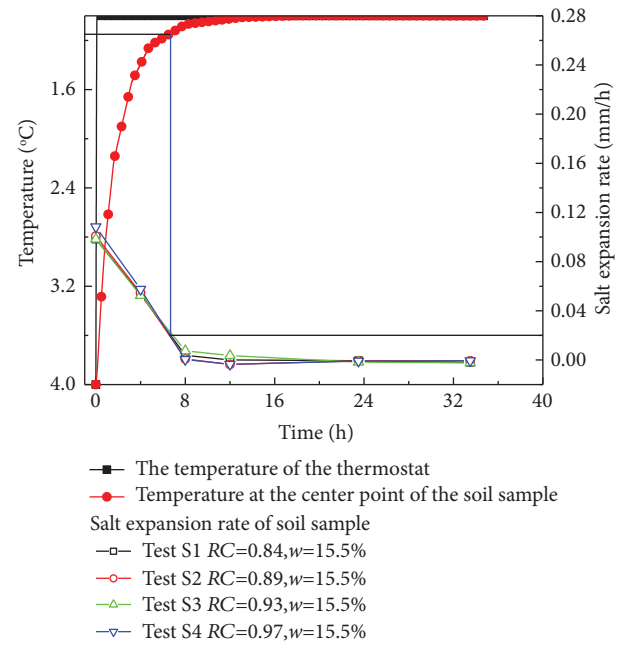

Figure 14: Variation soil sample expansion rate with time at 1°C with a cooling rate of 1°C/min.

temperature and the initial ambient temperature. Taking the temperature completion rate of 95% (8.2°C) as the temperature stability standard and taking the salt expansion rate less than 0.02 mm/h as the deformation stability standard, the temperature curve and the salt expansion rate curve under this stable standard can be obtained. So the salt swelling and deformation stability time can be obtained. Similarly, Figures 14 and 16 show that the soil sample is deformed and stabilized at 4°C and then cooled to 1°C. In this case, the critical crystallization temperature of the soil sample is 4°C.

The salt expansion rate curve with a cooling rate of 1°C/min is more stable than the one with a cooling rate of 1°C/h, and the error is relatively small. The reasons are as follows: (1) When the time is fixed, the faster the cooling rate, the greater the soil sample's temperature change, the larger the corresponding crystallization amount, the greater the salt expansion, and the smaller the relative error during measurement. (2) The sample's expansion height with a cooling rate of 1°C/min is measured every 4 hours, and the sample with a cooling rate of 1°C/h is measured every two hours. When the crystallization is not completed, the longer the measurement interval, the more considerable the amount of crystallization, the larger the salt expansion, and the smaller the relative error during

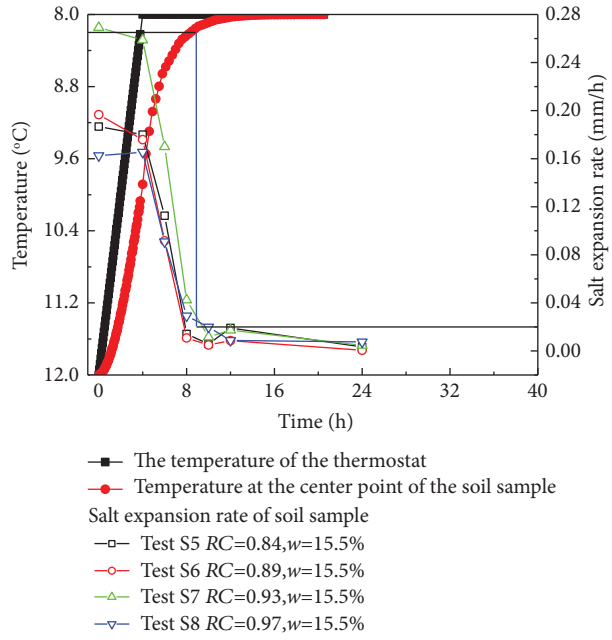

Figure 15: Soil sample swelling rate versus time at 8°C with a cooling rate of 1°C/h.

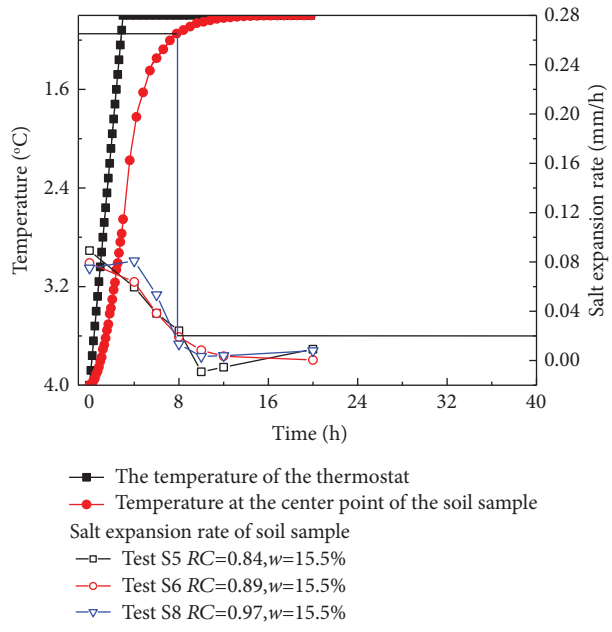

Figure 16: Variation soil sample expansion rate with time at 1°C with a cooling rate of 1°C/h.

measurement; the smaller the number of measurements, the more minor the disturbance to the sample and the smaller the error.

The variation curve of the sample's expansion rate with time under the liquid bath condition is shown in Figure 17. Under the temperature gradient, 20°C ⟶ 12°C ⟶ 8°C ⟶ 4°C ⟶ 1°C, taking the expansion rate less than 0.2 mL/h as the deformation stability standard, the deformation stability time is 0.86 h, 0.50 h, 0.72 h, and 0.67 h, respectively. After taking the average value, the deformation stability time is 0.7 h.

It can be obtained from Figures 13–17 that taking the expansion rate less than 0.02 mm/h as the deformation stability standard, when the incubator's cooling rate is 1°C/min and 1°C/h, the deformation stability time is 7 h and 10 h. Under the liquid bath condition, taking the expansion rate less than 0.2 mL/h as the deformation stability standard, the deformation stabilization time is 0.7 h. It can be obtained

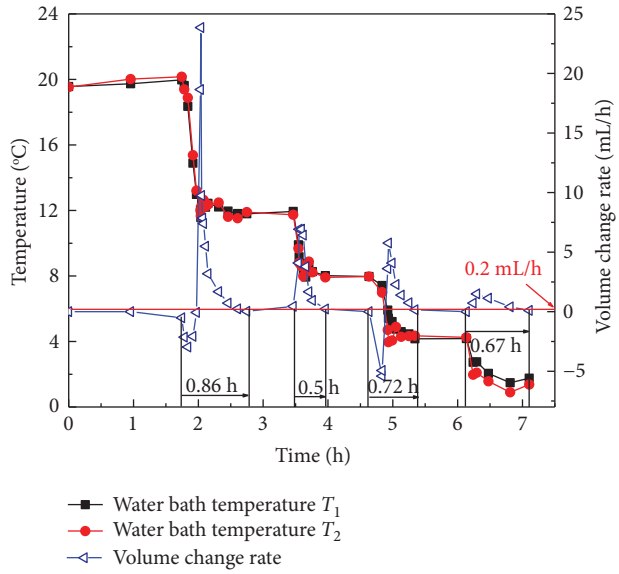

Figure 17: Variation curve of sample's expansion rate with time under the liquid bath condition.

that the test efficiency under liquid bath conditions is 10 times higher than that under air bath conditions.

4. Numerical Simulations on the Thermal Equilibrium Time

From Section 3, it can be concluded that the temperature of the sample is synchronized with the development of deformation; therefore, the salt expansion and deformation stability time of the sample can be obtained according to the temperature stabilization time of the sample. It is necessary to determine the reliability of the numerical simulation. This research establishes a numerical model based on the sample's actual size and the actual physical parameters of the sample and compares the numerical simulation results with the actual measured values.

4.1. Numerical Simulation Method. A two-dimensional rotating model is used to establish a cylindrical specimen. The study uses a triangular mesh and controls the mesh through physics.

According to the soil type, dry density, and moisture content of the salt expansion test sample, refer to Wang et al. [44] and Bai et al. [45, 46], determine the model's parameters, and determine the heat transfer coefficient based on the cooling method. The sample's dry density is 1700 kg/m^3. The sample's moisture content is 15.50%. The thermal conductivity and the specific heat capacity are 0.8 W/(m·K) and 1600 J/(kg·K), respectively. In the air bath conditions, the heat transfer coefficient is 5 W/cm^2·K. In the liquid bath conditions, the heat transfer coefficient is 200 W/cm^2·K.

A simple example is used to verify the reliability of the numerical model. The ambient temperature is 12°C, the initial temperature of the sample is 25°C, and the sample size at 0.2 h is $r = 8.95$ cm and $h = 11.59$ cm. The temperature simulation cloud diagram of the sample is shown in Figure 18.

The temperature distribution of the sample at this moment can be obtained from Figure 18, and the temperature at the center point of the sample and the maximum temperature of the sample at this time can be read. The temperature statistics in the following text refer to the temperature at the center point of the sample.

The numerical simulation cooling process is consistent with the actual soil sample cooling process. The initial temperature of the sample is 25°C, and the temperature is reduced according to 25°C ⟶ 12°C ⟶ 8°C ⟶ 4°C. The temperature of the center point of the sample is collected every 0.1 h during cooling.

Test process: first, we put the sample in a constant temperature box and set the temperature of the constant temperature box to 25°C ⟶ 12°C ⟶ 8°C ⟶ 4°C cooling gradient. The cooling rate of the constant temperature box is 1°C/min. Enough time is distributed at each temperature level to ensure the sample temperature reaches the ambient temperature. Then, we place the PT100 temperature sensor in the center of the soil sample and use DT85 to collect the soil sample's center temperature in real-time (collection frequency: 1 min/time). The collective result is shown in Figure 19.

The numerical simulation results are in good agreement with the experimental results, as shown in Figure 19. During the test, due to the exothermic of salt crystallization, the sample temperature curve with time has slight fluctuations, and the influence of salt crystallization is not considered in the numerical simulation process, resulting in error.

Numerical simulation tests for samples of different sizes under the same cooling conditions are carried out to determine the temperature stabilization time. The parameters of the numerical simulation are mentioned in Section 4.1. The test plan is shown in Table 3.

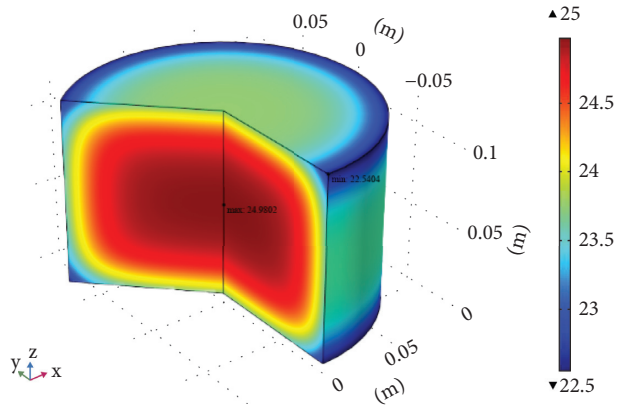

Figure 18: Sample temperature cloud diagram.

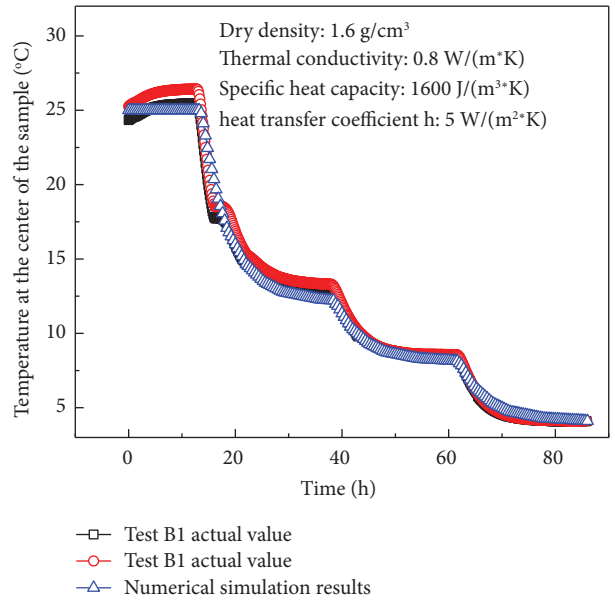

Figure 19: Soil temperature with time in the cooling stage.

Table 3: Numerical test plan.

Test number	Radius r (cm)	Height h (cm)	Cooling method
Test 1	3.09	4.00	
Test 2	6.18	8.00	
Test 3	8.95	11.59	
Test 4	30.90	40.00	
Test 5	10.00	20.00	Air bath
Test 6	20.00	20.00	
Test 7	20.00	40.00	
Test 8	30.00	60.00	
Test 9	40.00	80.00	
Test 10	1.96	8.00	
Test 11	2.50	10.00	
Test 12	10.00	20.00	
Test 13	20.00	20.00	
Test 14	20.00	40.00	Liquid bath
Test 15	30.00	60.00	
Test 16	40.00	80.00	
Test 17	25.00	80.00	

The numerical simulation cooling process is consistent with the actual soil sample cooling process. The initial temperature of the sample is 25°C, and the temperature is reduced according to 25°C ⟶ 12°C ⟶ 8°C ⟶ 4°C ⟶ 1°C. The temperature of the center point of the sample is collected every 0.1 h during cooling.

4.2. Numerical Calculation Results. The numerical simulation process and parameters are shown in Section 4.1. Only the sample size is changed, and the sample's center point's temperature value is recorded every 0.1 h. The curve of the temperature of the sample's center point with time is shown in Figure 20.

4.3. Thermal Equilibrium Time Analysis. Determining the sample's temperature stability standard is necessary for determining its stabilization time. Therefore, the tentative temperature completion rate (0.99), the temperature

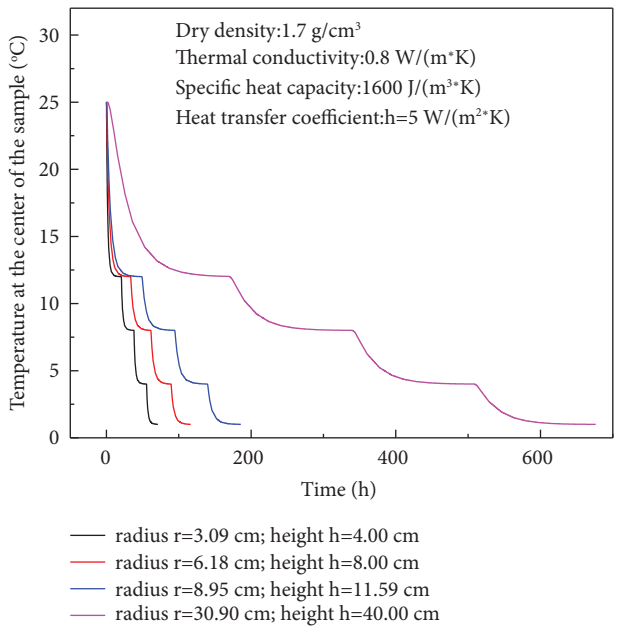

Figure 20: The temperature at the sample center changes with time during the cooling process.

completion rate (0.95), and the error of 0.1°C are uniformly controlled for the test of different sizes. Finally, comprehensively considering the test temperature control accuracy, the acceptable temperature error range, and the test efficiency, the sample's temperature stabilization time with different sizes and different temperature gradients is given. The details are shown in Table 4.

When the cooling conditions are the same and the sample size is different, the temperature gradient inside the sample is different, and the temperature equilibrium time is also different. The effective radius r_s characterizes different sizes, and its expression is

$$r_s = \frac{3V}{S}, \tag{1}$$

where V is the sample volume and S is the sample surface area.

The temperature completion rate of 95% is taken as the sample temperature's stability standard, comprehensively considering the test efficiency and the test accuracy. As the temperature stabilization time is minimal when the temperature difference differs, the average value of the temperature stabilization time at all levels is taken as the temperature stabilization time of the sample. The relationship between the sample's temperature stabilization time and the effective radius is shown in Figure 21.

4.4. A Determination Method on Thermal Equilibrium Time. The temperature completion rate of 95% is taken as the sample temperature's stability standard, comprehensively considering the test efficiency and test accuracy. Results from Section 3.4 indicate that when the temperature completion rate reaches 95%, the equilibrium time is the same as the deformation stability standard.

Based on the test results in Figure 21, a formula for calculating the thermal equilibrium time (or the salt expansion equilibrium time) can be established as follows.

In air bath conditions,

$$t_{e,\text{air}} = 0.05r_s^2 + 2.02r_s. \tag{2}$$

In liquid bath conditions,

$$t_{e,\text{liquid}} = 0.06r_s^2 + 0.02r_s, \tag{3}$$

where $t_{e,\text{air}}$ and $t_{e,\text{liquid}}$ are the time and r_s is the effective radius.

The list of deformation stability time of samples with different sizes and different cooling methods is shown in Table 5.

5. A Standard Experimental Procedure for Salt Expansion Test

5.1. Test Process Description. Under closed conditions, when there is a temperature difference between the soil sample and the environment, as time increases, the soil temperature decreases, and sodium sulfate's solubility decreases. The sodium sulfate in the pore solution crystallizes to form $Na_2SO_4{\cdot}10H_20$, and the volume of the soil expands. Therefore, the salt expansion process refers to when the volume changes with time and finally stabilizes after the temperature difference between the soil sample and the environment is sufficiently small. This process is similar to the consolidation process. The salt expansion is temperature-driven salt crystallization, which leads to volume development over time. The consolidation involves the water out driven by load and the volume development over time. Thus, the one-dimensional salt expansion test method can be compared to the consolidation test method [43].

Table 4: Stability standard and stabilization time of sample temperature under gas bath conditions.

Initial temperature of a sample	Ambient temperature	Temperature difference	Control standard	Judgment temperature	Stable time (test 1)	Stable time (test 2)	Stable time (test 3)	Stable time (test 4)
25	12	13	0.99	12.13	9.9	20.0	30.0	130.1
12	8	4	0.99	8.04	11.6	20.6	33.0	130.3
8	4	4	0.99	4.04	11.5	20.6	33.0	130.3
4	1	3	0.99	1.03	11.5	20.6	32.7	127.5
25	12	13	**0.95**	12.65	**5.8**	**11.8**	**18.5**	**86.2**
12	8	4	**0.95**	8.20	**6.6**	**13.3**	**20.5**	**88.6**
8	4	4	**0.95**	4.20	**6.5**	**13.3**	**20.9**	**88.6**
4	1	3	**0.95**	1.15	**6.5**	**13.2**	**19.9**	**88.6**
25	12	13	0.1°C	12.10	10.3	20.9	31.2	135.7
12	8	4	0.1°C	8.10	8.0	16.5	24.9	106.9
8	4	4	0.1°C	4.10	7.9	16.5	25.4	106.9
4	1	3	0.1°C	1.10	7.4	14.6	24.2	99.6

Note. The temperature unit in the table is °C; the unit of time in the table is the hour (*h*).

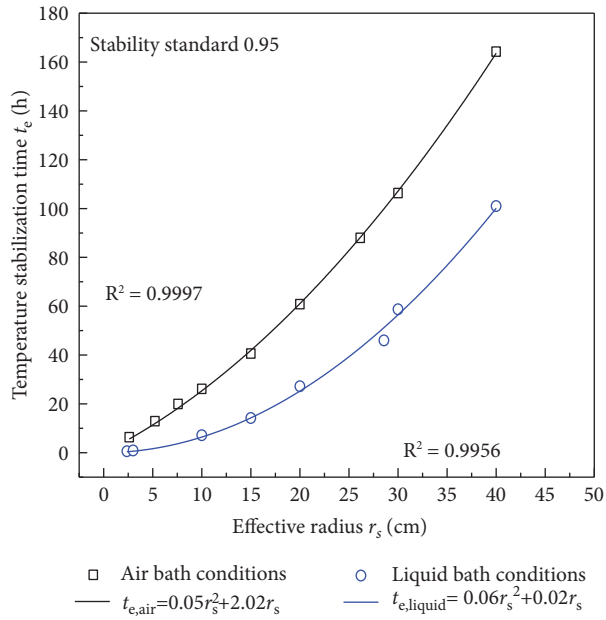

Figure 21: The relationship between the temperature stabilization time and the effective radius.

Table 5: List of deformation stability time.

Experiment type	Sample size	Equivalent radius (cm)	Cooling method	Balance time (h)
Confined one-dimensional salt expansion test	D = 6.18 cm and H = 4.00 cm	2.61	Gas bath	7
	D = 17.90 cm and H = 11.59 cm	7.59		20
	D = 61.80 cm and H = 40.00 cm	26.10		88
Three-dimensional salt expansion test	D = 3.91 cm and H = 8.00 cm	2.37	Liquid bath	0.5
	D = 5.00 cm and H = 10.00 cm	3.00		0.7
	D = 50.00 cm and H = 80.00 cm	28.56		46

For this, the following test procedures are adopted:

General provisions of one-dimensional salt expansion test method: the soil sample should be fine-grained soil with moisture content less than the liquid limit moisture content.

The experimental equipment should meet the following requirements: (a) salt expansion container: cutting ring (height 4 cm and diameter 6.18 cm) and constant temperature box (temperature control range −10–65°C and temperature fluctuation +0.1°C); (b) deformation measuring equipment: vernier caliper (graduation value 0.01 mm).

The one-dimensional salt expansion test should be carried out based on the following steps: (a) According to the project's needs, cut samples of undisturbed soil or prepare samples of disturbed soil with given density, water content, and salt content. The salt content is thoroughly mixed with soil in the form of salt solution to prepare samples. The ambient temperature during the sample preparation is not lower than the temperature corresponding to the salt solution's solubility to ensure that the salt does not crystallize during the sample preparation process. The preparation method shall be carried out according to the standard geotechnical test methods. (b) Seal the sample well, and then put it in a thermostat for 24 h (set the thermostat temperature as the initial temperature of the test program). (c) Measure the height of the sample (divide the circumference of the cutting ring into three equal parts, and calculate the average of the three measurements), and weigh the sample mass. (d) Set the temperature of the incubator according to the test plan, and measure the height of the sample when the temperature is stable for 7 hours. (e) Change to the next temperature level (generally, the temperature interval is not less than 3°C) and repeat step "d" until all the test plan temperatures are completed.

5.2. Determination of Salt Expansion Rate. The measured height of the sample minus the height of the sample measured after curing for 24 h is regarded as the salt swelling height, which is recorded as $2h_{\max}$. The salt expansion test directly measures the sample's maximum expansion height; thereby, the salt expansion volume should be calculated according to the maximum expansion height, and the salt expansion volume is calculated by the following formula [47]:

$$\Delta V_1 = \int_0^{h_{\max}} \pi\left[(x-R)^2\right]\mathrm{d}y = \pi\int_0^{h_{\max}} \frac{(h_{\max}-y)}{h_{\max}}\mathrm{d}y = \frac{\left(\pi R^2 h_{\max}\right)}{2}, \tag{4}$$

where R is the radius of the cutting ring (3.09 cm); $h_{\max}$ is the maximum expansion height of the sample side.

When the cutting ring is freely expanded with no restriction at both ends, free expansion, assuming that the expansion at both ends is symmetrical, the total expansion volume is $2\Delta V_1$. In practical problems, it can be solved by using the relevant constitutive models [14, 15], analytical method, and numerical simulation [3, 46].

6. Conclusions

Through the laboratory and numerical tests, the following conclusions are obtained.

In the sulfate saline soil, the salt crystallization, the salt expansion, and the temperature equilibrium are cotranscriptionally occurring.

The salt expansion and deformation stability standard (expansion rate <0.02 mm/h) can be used to determine the equilibrium time, and the temperature stability standard (temperature completion rate >0.95%) can be used to determine the equilibrium time.

The sample's temperature stabilization time has a parabolic relationship with the sample's effective radius. The calculation formulas for the deformation stability time of samples using different sizes are derived.

Compared to the air bath, the liquid bath apparatus can significantly reduce the equilibrium time. For example, under air bath conditions, with the cutting ring sample (diameter 61.8 mm and height 40 mm), the one-dimensional salt expansion test's deformation stability time is 7 h. Under liquid bath conditions, with standard triaxial specimens (diameter 39.1 mm and height 80 mm), the deformation stability time is only 0.5 h.

Data Availability

Some or all data, models, or codes that support the findings of this study are available from the corresponding author upon reasonable request.

Conflicts of Interest

The authors declare that they have no conflicts of interest.

Acknowledgments

The authors would like to thank Professor Qi Ji-lin for his help and helpful discussion. This work was supported by the National Natural Science Foundation of China (51979002 and 52079003).

References

[1] C. H. Dong and X. M. Dong, "Tests on the dissolve settlement characteristics of sulphate saline soil," *Applied Mechanics and Materials*, vol. 361–363, pp. 1071–1074, 2013.

[2] B. Yuan, Z. Li, Z. Zhao, H. Ni, Z. Su, and Z. Li, "Experimental study of displacement field of layered soils surrounding laterally loaded pile based on Transparent Soil," *Journal of Soils and Sediments*, vol. 21, no. 9, pp. 3072–3083, 2021.

[3] C. Cui, K. Meng, C. Xu, Z. Liang, H. Li, and H. Pei, "Analytical solution for longitudinal vibration of a floating pile in saturated porous media based on a fictitious saturated soil pile model," *Computers and Geotechnics*, vol. 131, Article ID 103942, 2021.

[4] B. X. Yuan, Z. H. Li, Z. L. Su, Q. Z. Luo, M. J. Chen, and Z. Q. Zhao, "Sensitivity of multistage fill slope based on finite element model," *Advances in Civil Engineering*, vol. 2021, Article ID 6622936, 13 pages, 2021.

[5] Chinese Standard, *Technical Code for Building in saline Soil Regions (GB/T 50942-2014)*, China Planning Press, Beijing, China, 2014, in Chinese.

[6] Q. G. Ma, Y. M. Lai, and M. Y. Zhang, "Freezing-thawing behaviour of saline soil with various anti-saline measures," *European Journal of Environmental and Civil Engineering*, vol. 23, no. 10, pp. 1178–1202, 2019.

[7] Y. Lai, X. Wan, and M. Zhang, "An experimental study on the influence of cooling rates on salt expansion in sodium sulfate soils," *Cold Regions Science and Technology*, vol. 124, pp. 67–76, 2016.

[8] X. Wan, Z. You, H. Wen, and W. Crossley, "An experimental study of salt expansion in sodium saline soils under transient conditions," *Journal of Arid Land*, vol. 9, no. 6, pp. 865–878, 2017.

[9] X. Wan, E. Liu, E. Qiu, M. Qu, X. Zhao, and F. J. Nkiegaing, "Study on phase changes of ice and salt in saline soils," *Cold Regions Science and Technology*, vol. 172, Article ID 102988, 2020.

[10] B. Bai, L. Guo, and S. Han, "Pore pressure and consolidation of saturated silty clay induced by progressively heating/cooling," *Mechanics of Materials*, vol. 75, pp. 84–94, 2014.

[11] Z. Xiao, Y. M. Lai, and J. Zhang, "Method for calculating the liquid water fraction of saline soil during the freezing process," *Permafrost and Periglacial Processes*, vol. 32, no. 1, pp. 92–101, 2020.

[12] J. Fang, X. Li, J. Liu, C. Liu, Z. Liu, and Y. Ji, "The crystallization and salt expansion characteristics of a silty clay," *Cold Regions Science and Technology*, vol. 154, pp. 63–73, 2018.

[13] J. Zhang, Y. Lai, J. Li, and Y. Zhao, "Study on the influence of hydro-thermal-salt-mechanical interaction in saturated frozen sulfate saline soil based on crystallization kinetics," *International Journal of Heat and Mass Transfer*, vol. 146, Article ID 118868, 2020.

[14] B. Bai, R. Zhou, G. Cai, W. Hu, and G. Yang, "Coupled thermo-hydro-mechanical mechanism in view of the soil particle rearrangement of granular thermodynamics," *Computers and Geotechnics*, vol. 137, no. 8, Article ID 104272, 2021.

[15] B. Bai, G.-c. Yang, T. Li, and G.-s. Yang, "A thermodynamic constitutive model with temperature effect based on particle rearrangement for geomaterials," *Mechanics of Materials*, vol. 139, Article ID 103180, 2019.

[16] L. Wang, J. Liu, R. Feng, X. Zhang, and Z. Liu, "Experimental study on salt expansion characteristics of coarse-grained sulfate soils," *Journal of Cold Regions Engineering*, vol. 34, no. 2, Article ID 04020004, 2020.

[17] X. Wan, F. Gong, M. Qu, E. Qiu, and C. Zhong, "Experimental study of the salt transfer in a cold sodium sulfate soil," *KSCE Journal of Civil Engineering*, vol. 23, no. 4, pp. 1573–1585, 2019.

[18] D. Hunter, "Lime-Induced heave in sulfate-bearing clay soils," *Journal of geotechnical engineering*, vol. 114, no. 2, pp. 150–167, 1988.

[19] J. K. Mitchell and D. Dermatas, "Clay soil heave caused by lime-sulfate reactions," *ASTM*, vol. 1135, pp. 41–64, 1992.

[20] F. Padilla and J.-P. Villeneuve, "Modeling and experimental studies of frost heave including solute effects," *Cold Regions Science and Technology*, vol. 20, no. 2, pp. 183–194, 1992.

[21] S. L. Yang, W. Zhang, Y. Wen, and B. Li, "Salt expansion and lateral mechanical properties of fine-grained saline soil foundation in Xining basin," *Journal of Qinghai University*, vol. 35, no. 6, pp. 61–68, in Chinese, 2017.

[22] R. Tang, G. Zhou, J. Wang, G. Zhao, Z. Lai, and F. Jiu, "A new method for estimating salt expansion in saturated saline soils during cooling based on electrical conductivity," *Cold Regions Science and Technology*, vol. 170, Article ID 102943, 2020.

[23] S. Zhang, J. Zhang, Y. Gui, W. Chen, and Z. Dai, "Deformation properties of coarse-grained sulfate saline soil under the freeze-thaw-precipitation cycle," *Cold Regions Science and Technology*, vol. 177, Article ID 103121, 2020.

[24] B. Bai, T. Xu, Q. Nie, and P. Li, "Temperature-driven migration of heavy metal Pb2+ along with moisture movement in unsaturated soils," *International Journal of Heat and Mass Transfer*, vol. 153, Article ID 119573, 2020.

[25] B. Bai, Q. Nie, Y. Zhang, X. Wang, and W. Hu, "Cotransport of heavy metals and SiO2 particles at different temperatures by seepage," *Journal of Hydrology*, vol. 597, Article ID 125771, 2021.

[26] B. Bai, F. Long, D. Rao, and T. Xu, "The effect of temperature on the seepage transport of suspended particles in a porous medium," *Hydrological Processes*, vol. 31, no. 2, pp. 382–393, 2017.

[27] B. Bai, Q. Nie, H. Wu, and J. Hou, "The attachment-detachment mechanism of ionic/nanoscale/microscale substances on quartz sand in water," *Powder Technology*, vol. 394, pp. 1158–1168, 2021.

[28] W.-C. Cheng, X.-D. Bai, B. B. Sheil, G. Li, and F. Wang, "Identifying characteristics of pipejacking parameters to assess geological conditions using optimisation algorithm-based support vector machines," *Tunnelling and Underground Space Technology*, vol. 106, Article ID 103592, 2020.

[29] X.-D. Bai, W.-C. Cheng, B. B. Sheil, and G. Li, "Pipejacking clogging detection in soft alluvial deposits using machine learning algorithms," *Tunnelling and Underground Space Technology*, vol. 113, Article ID 103908, 2021.

[30] D. Rao and B. Bai, "Study of the factors influencing diffusive tortuosity based on pore-scale SPH simulation of granular soil," *Transport in Porous Media*, vol. 132, no. 2, pp. 333–353, 2020.

[31] B. Bai, D. Rao, T. Chang, and Z. Guo, "A nonlinear attachment-detachment model with adsorption hysteresis for suspension-colloidal transport in porous media," *Journal of Hydrology*, vol. 578, Article ID 124080, 2019.

[32] B. Bai, "Fluctuation responses of saturated porous media subjected to cyclic thermal loading," *Computers and Geotechnics*, vol. 33, no. 8, pp. 396–403, 2006.

[33] S. Q. Peng, F. Wang, and L. Fan, "Experimental study on influence of vaporous water on salt expansion of sulfate saline soil," *Advances in Civil Engineering*, vol. 2019, Article ID 6819460, 9 pages, 2019.

[34] H. Bing, P. He, and Y. Zhang, "Cyclic freeze-thaw as a mechanism for water and salt migration in soil," *Environmental Earth Sciences*, vol. 74, no. 1, pp. 675–681, 2015.

[35] D. Wu, X. Zhou, and X. Jiang, "Water and salt migration with phase change in saline soil during freezing and thawing processes," *Groundwater*, vol. 56, no. 5, pp. 742–752, 2018.

[36] R. Feng, L. Wu, and B. Wang, "Numerical simulation for temperature field and salt heave influential depth estimation in sulfate saline soil highway foundations," *International Journal of Geomechanics*, vol. 20, no. 10, Article ID 04020196, 2020.

[37] B. Bai and X. Shi, "Experimental study on the consolidation of saturated silty clay subjected to cyclic thermal loading," *Geomechanics and Engineering*, vol. 12, no. 4, pp. 707–721, 2017.

[38] P. Zhang, B. Bai, S. Jiang, P. Wang, and H. Li, "Transport and deposition of suspended particles in saturated porous media: effect of hydrodynamic forces and pore structure," *Water Supply*, vol. 16, no. 4, pp. 951–960, 2016.

[39] B. Yuan, Z. Li, Y. Chen et al., "Mechanical and microstructural properties of recycling granite residual soil reinforced with glass fiber and liquid-modified polyvinyl alcohol polymer," *Chemosphere*, vol. 286, Article ID 131652, 2022.

[40] W. Hu, W.-C. Cheng, S. Wen, and M. Mizanur Rahman, "Effects of chemical contamination on microscale structural characteristics of intact loess and resultant macroscale mechanical properties," *Catena*, vol. 203, Article ID 105361, 2021.

[41] M. Steiger, "Crystal growth in porous materials: influence of supersaturation and crystal size," *ÁlvarezDeBuergo*, vol. 1-2, pp. 245–251, 2006.

[42] W. L. Hu, W. C. Cheng, S. J. Wen, and K. Yuan, "Revealing the enhancement and degradation mechanisms affecting the performance of carbonate precipitation in EICP process," *Frontiers in Bioengineering and Biotechnology*, vol. 9, Article ID 750258, 2021.

[43] Chinese Standard, *Geotechnical Test Method Standard (GB/T 50123-2019)*, China Planning Press, Beijing, China, 2019, in Chinese.

[44] T. X. Wang, Z. C. Liu, and J. Lu, "Experimental study on coefficient of thermal conductivity and specific volume heat of loess," *Rock and Soil Mechanics*, vol. 28, no. 4, pp. 655–658, 2007, in Chinese.

[45] B. Bai, D. Rao, T. Xu, and P. Chen, "SPH-FDM boundary for the analysis of thermal process in homogeneous media with a discontinuous interface," *International Journal of Heat and Mass Transfer*, vol. 117, pp. 517–526, 2018.

[46] B. Bai and T. Li, "Irreversible consolidation problem of a saturated porothermoelastic spherical body with a spherical cavity," *Applied Mathematical Modelling*, vol. 37, no. 4, pp. 1973–1982, 2013.

[47] X. W. Zhao, X. Li, J. K. Liu, and Y. Zhang, "The effect of confining boundary on soil deformation in one dimensional frost heave tests and the theoretical volume correction," *Sciences in Cold and Arid Regions*, vol. 5, no. 5, pp. 587–590, 2013.